IEEE Access
Multidisciplinary | Rapid Review | Open Access Journal

Received March 24, 2021, accepted March 31, 2021, date of publication April 12, 2021, date of current version April 19, 2021.

Digital Object Identifier 10.1109/ACCESS.2021.3072481

Beamforming and Reflection Coefficient Control for Multiantenna Backscatter Communication With Nonorthogonal Multiple Access

GERARDO SACARELO[1] AND YUN HEE KIM[1,2], (Senior Member, IEEE)
[1]Department of Electronics and Information Convergence Engineering, Kyung Hee University, Yongin 17104, South Korea
[2]Department of Electronic Engineering, Kyung Hee University, Yongin 17104, South Korea

Corresponding author: Yun Hee Kim (yheekim@khu.ac.kr)

This work was supported by the National Research Foundation of Korea (NRF) through the Korean Government under Grant 2018R1D1A1B07045515 and Grant 2021R1A2C1005869.

ABSTRACT For ultralow-power Internet of Things, we consider a monostatic multiantenna backscatter communication network (MBCN) supporting massive devices through nonorthogonal multiple access (NOMA) over space division multiple access (SDMA). For the network, we optimize the transmit beamforming (BF) for signal excitation of a reader, reflection coefficients of devices for backscattering and energy harvesting, and receive BF for information decoding at the reader toward the maximum fairness in data collection. We first show that the optimization problem for the MBCN without successive interference cancellation (SIC) has a similarity with the problem considered for a wireless power communication network but the conventional algorithm is not applicable to the MBCN with SIC. Thus, we propose a new alternating optimization algorithm that is applicable to both problems with and without SIC at a lower complexity. Simulation results show that the proposed algorithm provides a remarkable gain over the conventional one for the MBCN with SIC while exhibiting a similar performance for the MBCN without SIC. In addition, NOMA/SDMA enhanced by the proposed algorithm increases the minimum system throughput as well as the total energy harvested in the network by utilizing limited resources more effectively for a larger number of devices.

INDEX TERMS Backscatter communication, beamforming, nonorthogonal multiple access, reflection coefficient, successive interference cancellation.

I. INTRODUCTION

Proliferation of Internet of Things (IoT) is expected to surge for autonomous and intelligent controls of various things while imposing diverse requirements on communication devices and networks [1], [2]. One of the key requirements is to prolong the lifetime of IoT devices without frequent battery replacements and even without a battery installation to reduce a form factor. To meet this requirement to some degree, remote wireless power transfer to IoT devices through a radio frequency (RF) signal has been addressed into wireless communications in a form of simultaneous wireless information and power transfer (SWIPT) [3]–[5] and wireless power communication networking (WPCN) [6], [7]. SWIPT provides energy and data flows in the same direction, typically in the downlink, whilst WPCN provides them in different directions such as energy flow in the downlink and data flow in the uplink. To improve the power-efficiency of IoT devices further, backscatter modulation, sending data by reflecting a carrier signal excited from another source [8], [9], has been addressed into recent IoT applications [10], [11], where IoT devices are exempt from installing power-consuming active RF circuits and even harvest the energy from the incident carrier.

Such backscatter communication (BackCom) networks are classified according to a source emitting a carrier signal: monostatic if the source is also a reader decoding the backscatter signals [12]–[19], bistatic if the source and the reader are different entities [20], and ambient if the source is a transmitter of another network in the vicinity of the reader [21]–[23]. In the networks, backscatter IoT devices (BDs) may reflect the incident carrier signal for backscatter modulation fully or in part or harvest the energy from the carrier signal. The monostatic, bistatic, ambient BackCom networks have been developed in various aspects to exploit their own advantages with some variations, and new types of BackCom

The associate editor coordinating the review of this manuscript and approving it for publication was Adao Silva.

networks have emerged such as a symbiotic radio performing cooperative ambient BackCom [24] and a hybrid BD generating an RF carrier and backscattering an incident RF signal as well [25].

This article focuses on monostatic BackCom with a full-duplex reader and multiple BDs as in [12], [15], [16], [18], [19] that excites the signals to the BDs in the downlink for reflection and energy harvesting and collects the data from the reflected signals in the uplink. The monostatic BackCom has a resemblance to a cellular network suitable for centralized resource allocation and optimization in collecting data from massive IoT devices.

A. RELATED WORKS

To date, several multiple access (MA) schemes have been applied to the monostatic BackCom and their performances have been optimized from different aspects. For a single-antenna reader, time division multiple access (TDMA) protocols have been designed to maximize the throughput via time allocation [15] and multisine waveforms for an excitation signal have been optimized to improve the signal-to-interference-plus-noise ratio (SINR)-energy tradeoff of on–off backscatter modulation [16]. For a *multiantenna* reader, the transmit beamforming (BF) has been optimized taking into account channel estimation using backscatter pilot symbols [12]. Later, sum throughput and throughput fairness have been optimized in space division multiple access (SDMA) by optimizing the transmit BF and receive BF at the reader [18], [19].

In the meantime, nonorthogonal multiple access (NOMA) has received a huge attention recently as a promising technology of accommodating high data rate and massive connection of devices in a limited wireless resource [26], [27]. NOMA allows a simultaneous transmission of signals more than those supportable in an orthogonal manner through successive interference cancellation (SIC) and power allocation. Our concern is limited to the uplink NOMA for data collection that can be implemented with SIC at the receiver and power allocation at the transmitters although power allocation is not mandatory in the uplink. The uplink NOMA has been studied with a single-antenna receiver [26]–[29] and then with a *multiantenna* receiver [30]–[32], which have also been incorporated into WPCN and BackCom for massive connection of power-hungry IoT devices [24], [33]–[40]. It should be noted that SWIPT providing data and energy flows in the same direction has been studied for the downlink in general without discussing the uplink [3]–[5]. Although a few recent studies have dealt with SWIPT in the downlink and data collection in the uplink jointly [41], [42], NOMA in SWIPT was considered only in the downlink [43].

We now first review on WPCN with NOMA in which a hybrid access point (HAP) collects data from IoT devices through uplink NOMA after performing wireless power transfer (WPT) to the devices in the downlink. Initial studies have considered a *single-antenna* HAP for which time allocation to the downlink and uplink phases and power allocation in the uplink NOMA were optimized to maximize the sum throughput or energy efficiency [33]–[35]. Later, a *multiantenna* HAP has been considered to overlay NOMA over SDMA [36], [37], but only the power allocation in the downlink WPT and time allocation have been optimized for a given transmit and receive BF and only the receive BF and power control have been optimized with isotropic transmit BF [37].

We next review on BackCom with NOMA, where a reader collects data from multiple BDs via backscattter modulation. For monostatic BackCom of our concern, the uplink NOMA was considered with a *single-antenna* reader only, where the constant reflection coefficients of BDs have been chosen to optimize the average number of successfully decoded bits [38]. NOMA over TDMA has been considered for bistatic BackCom with a single-antenna source and a *multiantenna* reader, where the minimum throughput has been maximized by optimizing time allocation for TDMA and reflection coefficients for NOMA for a given receive BF [39]. NOMA-enhanced protocols have also been considered for cooperative ambient BackCom but with single-antenna transmitters and receivers [24], [40].

To the best of our knowledge, the studies that have addressed uplink NOMA to SDMA in WPCN and BackCom did not consider an optimization of the transmit and receive BF of multiantenna transceivers and power control of IoT devices jointly for rate fairness.

B. CONTRIBUTIONS

In this context, we consider a monostatic multiantenna BackCom network (MBCN) that supports multiple BDs in uplink NOMA over SDMA, where SDMA with SIC was considered as a special case. The unique features and contributions of this article are as follows:

- We consider the problem of optimizing the transmit BF for excitation signals, the receive BF for data collection via backscatter modulation, and the reflection coefficients of the BDs jointly toward the maximum fairness for the MBCN with uplink NOMA. This kind of joint optimization problem has not been studied for BackCom networks with NOMA for which a single-antenna transmitter without transmit BF was considered [24], [38]–[40]. Even for a similar network as WPCN, NOMA has been studied with a single-antenna HAP [33]–[35] or a multi-antenna HAP employing a fixed transmit BF [36], [37].
- We first show that the problem for the MBCN *without SIC* has a similarity with the problem tackled for a WPCN based on SDMA [44] for which an alternating optimization algorithm was derived from the balanced SINR condition. We then show that our problem with SIC cannot be solved optimally with the algorithm proposed in [44] due to the SIC operation leading to the SINR imbalance among the BDs.
- For the MBCN with NOMA, we propose a new alternating optimization algorithm of the receive BF, transmit

BF, and reflection coefficient that adopts the conditionally optimal receive BF obtained explicitly, transmit BF optimization via successive convex approximation (SCA), and two-step reflection coefficient optimization. The proposed algorithm reduces the complexity of the existing algorithm based on the spectral radius minimization for both NOMA and SDMA without a performance degradation [44], and also provides a remarkable gain in the rate performance over the existing algorithm for NOMA.

- We also show that the reflection coefficient optimization method unique in the proposed algorithm increases the energy harvested at the BDs compared with the power control method in [37] for both cases of linear and nonlinear energy harvesting models [5].

The remainder of the article is organized as follows: Section II presents the system model of the monostatic MBCN and formulates a max–min rate optimization problem for the MBCN without and with SIC. Some resemblance between the problem herein and an existing problem for WPCN is shown in Section III along with different aspects that make the existing algorithm inapplicable. Section IV proposes an alternating optimization algorithm for our problem that is also applicable to the existing problem. Simulation results to validate the algorithm and advantages of NOMA are provided in Section V. Finally, conclusions are made in Section VI.

Notation: Lowercase and uppercase bold letters are used to represent column vectors and matrices, respectively. The set of $n \times m$ complex-valued matrices is denoted by $\mathbb{C}^{n\times m}$ with $\mathbb{C}^n = \mathbb{C}^{n\times 1}$, and the set of length-$n$ vectors with nonnegative real-valued entries is denoted by $\mathbb{R}^n_+$. The all-zero and all-one vectors of length-n are denoted by $\mathbf{0}_n$ and $\mathbf{1}_n$, respectively. In addition, $\boldsymbol{I}_n$ denotes the $n \times n$ identity matrix and diag($\boldsymbol{a}$) denotes the diagonal matrix with diagonal elements given by the elements of a vector $\boldsymbol{a}$. The inequality symbol $\leq$ implies the entry-wise inequality if it is applied to two vectors of the same length. $\mathbb{E}[\cdot]$ is used to denote the expectation, $\mathcal{CN}(\boldsymbol{\mu}, \boldsymbol{\Sigma})$ is used to represent a complex Gaussian distribution with mean vector $\boldsymbol{\mu}$ and covariance matrix $\boldsymbol{\Sigma}$, and $\sim$ is used to signify "distributed as."

II. SYSTEM MODEL AND PROBLEM FORMULATION

We consider a monostatic MBCN described in Fig. 1, where a full-duplex reader supports K BDs $\{D_k\}_{k=1}^K$. The reader is equipped with M antennas, while each BD is equipped with a single antenna. In addition, the network supports both cases of $K > M$ and $K \leq M$ by addressing SIC at the reader. We assume that the channel reciprocity holds for the channel between the reader and a BD and each channel experience independent flat Rayleigh fading. The baseband equivalent channel between the reader and D_k is denoted by $\boldsymbol{h}_k \sim \mathcal{CN}(\mathbf{0}_M, \omega_k \boldsymbol{I}_M)$, where $\omega_k = \omega_0\, d_k^{-\nu}$ represents the path loss at distance d_k with reference path loss ω_0 and path loss exponent ν.

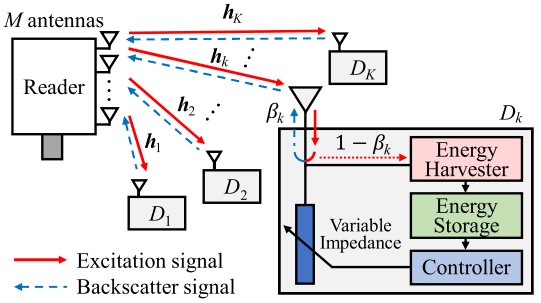

FIGURE 1. Monostatic MBCN with a multiantenna reader and multiple BDs.

The reader transmits the excitation signal $\sqrt{P_T}\boldsymbol{v}$ over M antennas, where P_T is the transmit power and $\boldsymbol{v} \in \mathbb{C}^M$ is the transmit BF subject to $\|\boldsymbol{v}\|^2 \leq 1$. The incident signal at D_k is then expressed as $\sqrt{P_T}\boldsymbol{h}_k^T\boldsymbol{v}$, of which the portion is reflected by varying the impedance load of the BD with a modulation symbol being embedded and the other portion is utilized for energy harvesting as shown in Fig. 1. The backscatter signal at D_k is expressed as

$$x_k = \sqrt{P_T\beta_k}\boldsymbol{h}_k^T\boldsymbol{v}s_k, \tag{1}$$

where $\beta_k \in [0, 1]$ is the reflection coefficient of D_k and s_k is the modulation symbol embedded in the backscatter signal subject to $\mathbb{E}[|s_k|^2] = 1$.

The harvested energy at D_k per unit time is expressed as

$$E_k = \Phi_{\mathfrak{h}}(P_T(1-\beta_k)|\boldsymbol{h}_k^T\boldsymbol{v}|^2), \tag{2}$$

where $\Phi_{\mathfrak{h}}()$ is the input-output power function of the EH circuit for $\mathfrak{h} \in \{L, N\}$. We consider not only a linear EH (LEH) model described as

$$\Phi_L(p) = \eta_{\text{eff}}p \tag{3}$$

with EH efficiency η_{eff} but also a practical nonlinear EH (NLEH) model described by a sigmoid-like function as

$$\Phi_N(p) = P_{sat}\frac{1-e^{-ap}}{1+e^{-a(p-p_c)}}, \tag{4}$$

where P_{sat} is the output saturation power, a is the positive charging rate, and p_c is the curvature point. Here, the NLEH function (4) is a equivalent form of that in [5] that is expressed more explicitly.

The full-duplex reader receives the backscatter signals while transmitting the excitation signal, where the self-interference from the excitation signal is assumed to be canceled perfectly as in [12], [15]–[18], [38]. The backscatter signals received at the reader are then given as follows:

$$\boldsymbol{y} = \sum_{l=1}^{K}\sqrt{P_T\beta_l}\boldsymbol{h}_l\boldsymbol{h}_l^T\boldsymbol{v}s_l + \boldsymbol{n}, \tag{5}$$

where $\boldsymbol{n} \sim \mathcal{CN}(\mathbf{0}_M, \sigma^2\boldsymbol{I}_M)$ is the complex Gaussian noise vector at the antennas of the reader. Without SIC, the signal

for detection of s_k is given by

$$z_k = \boldsymbol{w}_k^H \boldsymbol{y} = \sum_{l=1}^{K} \sqrt{P_T \beta_l} \boldsymbol{w}_k^H \boldsymbol{h}_l \boldsymbol{h}_l^T \boldsymbol{v} s_l + \boldsymbol{w}_k^H \boldsymbol{n}, \tag{6}$$

where $\boldsymbol{w}_k \in \mathbb{C}^M$ is the receive BF for D_k.

This paper addresses SIC for symbol detection with the receive BF which is performed in the order of the BD index without a loss of generality. The signal after the $(k-1)$th symbol being canceled is given by

$$\hat{\boldsymbol{y}}_k = \sum_{l=k}^{K} \sqrt{P_T \beta_k} \boldsymbol{h}_l \boldsymbol{h}_l^T \boldsymbol{v} s_l + \boldsymbol{n}. \tag{7}$$

The receive BF $\boldsymbol{w}_k$ is applied to (7) as

$$\hat{z}_k = \boldsymbol{w}_k^H \hat{\boldsymbol{y}}_k = \sum_{l=k}^{K} \sqrt{P_T \beta_k} \boldsymbol{w}_k^H \boldsymbol{h}_l \boldsymbol{h}_l^T \boldsymbol{v} s_l + \boldsymbol{w}_k^H \boldsymbol{n} \tag{8}$$

to detect symbol s_k from $k = 1$ to K sequentially.

The SINR experienced in detecting symbol s_k without and with SIC is expressed in a unified form as

$$\gamma_k = \frac{P_T \beta_k |\boldsymbol{w}_k^H \boldsymbol{h}_k|^2 |\boldsymbol{h}_k^T \boldsymbol{v}|^2}{\sum\limits_{l \in \mathfrak{I}_k}^{K} P_T \beta_l |\boldsymbol{w}_k^H \boldsymbol{h}_l \boldsymbol{h}_l^T \boldsymbol{v}|^2 + \sigma^2 \|\boldsymbol{w}_k\|^2} \tag{9}$$

from (6) and (8), where $\mathfrak{I}_k$ is the index set of BDs interfering to D_k given as follows:

$$\mathfrak{I}_k = \mathfrak{O}_k \triangleq \{1, 2, \cdots, K\} - \{k\} \tag{10}$$

without SIC and

$$\mathfrak{I}_k = \mathfrak{N}_k \triangleq \{k+1, k+2, \cdots, K\} \tag{11}$$

with SIC.

III. PROBLEM FORMULATION AND ANALYSIS

We aim at maximizing the minimum rate of the BDs to collect data with fairness by optimizing the receive BF $\boldsymbol{W} = [\boldsymbol{w}_1, \boldsymbol{w}_2, \cdots, \boldsymbol{w}_K]$, the transmit BF $\boldsymbol{v}$, and reflection coefficient $\boldsymbol{\beta} = [\beta_1, \beta_2, \cdots, \beta_K]^T$ jointly. With the achievable rate

$$R_k = \log_2(1 + \gamma_k) \tag{12}$$

from BD D_k to the reader, the optimization problem can be formulated as

$$\max_{\boldsymbol{W} \in \mathbb{C}^{M \times K}, \boldsymbol{v} \in \mathbb{C}^M, \boldsymbol{\beta} \in \mathbb{R}_+^K} \left\{ \min_{1 \le k \le K} \log_2(1 + \gamma_k) \right\} \tag{13a}$$

$$\text{subject to } \|\boldsymbol{v}\|^2 \le 1, \tag{13b}$$

$$\boldsymbol{\beta} \le 1 \tag{13c}$$

of which the optimal value and variables are denoted by $R_{\min}^o$ and $(\boldsymbol{W}^o, \boldsymbol{v}^o, \boldsymbol{\beta}^o)$, respectively.

The optimal variables for the max–min rate problem (13) can be obtained by the following max–min SINR problem

$$\max_{\boldsymbol{W} \in \mathbb{C}^{M \times K}, \boldsymbol{v} \in \mathbb{C}^M, \boldsymbol{\beta} \in \mathbb{R}_+^K} \left\{ \min_{1 \le k \le K} \gamma_k \right\} \tag{14a}$$

$$\text{subject to (13b) and (13c)} \tag{14b}$$

due to the monotonically increasing property of the log function. We now show that the problem (14) without SIC is equivalent to the max–min SINR problem tackled in [44], but the problem (14) with SIC cannot be solved by the algorithm proposed in [44].

For this purpose, we apply a change of variables to reflection coefficients as

$$p_k = P_T \beta_k |\boldsymbol{h}_k^T \boldsymbol{v}|^2, \quad k = 1, 2, \cdots, K, \tag{15}$$

which is equivalent to the power of the reflected signals at the BDs. We then transform (14) with $\boldsymbol{p} = [p_1, p_2, \cdots, p_K]^T$ into

$$\max_{\boldsymbol{W} \in \mathbb{C}^{M \times K} \boldsymbol{v} \in \mathbb{C}^M, \boldsymbol{p} \in \mathbb{R}_+^K} \left\{ \min_{1 \le k \le K} \gamma_k \right\} \tag{16a}$$

$$\text{subject to } \|\boldsymbol{v}\|^2 \le 1, \tag{16b}$$

$$p_k \le P_T |\boldsymbol{h}_k^T \boldsymbol{v}|^2, \ \forall k, \tag{16c}$$

where the objective function is rewritten from (9) as follows:

$$\gamma_k = \frac{p_k |\boldsymbol{w}_k^H \boldsymbol{h}_k|^2}{\sum\limits_{l \in \mathfrak{I}_k} p_l |\boldsymbol{w}_k^H \boldsymbol{h}_l|^2 + \sigma^2 \|\boldsymbol{w}_k\|^2}. \tag{17}$$

It is now obvious that the problem (16) without SIC ($\mathfrak{I}_k = \mathfrak{O}_k$) takes a similar form with the problem solved for the WPCN [44] that optimized the energy BF in the downlink wireless power transfer phase, the receive BF for the uplink phase in SDMA, and the transmit power of devices transmitting the information with the harvested energy for a given time allocation to the downlink and uplink phases. Thus, we may apply the alternating optimization algorithm proposed in [44] that iteratively optimizes $\boldsymbol{W}$, $\boldsymbol{v}$, and $\boldsymbol{p}$, based on the spectral radius minimization (SRM) problem. The SRM-based algorithm relies on the balanced SINR condition observed in the power allocation problem for the transmit BF and receive BF fixed. Specifically, for a given $\boldsymbol{W} = \tilde{\boldsymbol{W}} = [\tilde{\boldsymbol{w}}_1, \tilde{\boldsymbol{w}}_2, \cdots, \tilde{\boldsymbol{w}}_K]$ and $\boldsymbol{v} = \tilde{\boldsymbol{v}}$, (16) becomes a power allocation problem

$$\max_{\boldsymbol{p} \in \mathbb{R}_+^K} \min_{1 \le k \le K} \gamma_k = \frac{p_k |\tilde{\boldsymbol{w}}_k^H \boldsymbol{h}_k|^2}{\sum\limits_{l \in \mathfrak{I}_k} p_l |\tilde{\boldsymbol{w}}_k^H \boldsymbol{h}_l|^2 + \sigma^2 \|\tilde{\boldsymbol{w}}_k\|^2} \tag{18a}$$

$$\text{subject to } p_k \le P_T |\boldsymbol{h}_k^T \tilde{\boldsymbol{v}}|^2, \forall k \tag{18b}$$

of which the optimal solution without SIC ($\mathfrak{I}_k = \mathfrak{O}_k$) is attained when the SINRs are equal as $\gamma_1 = \gamma_2 = \cdots = \gamma_K$. However, the balanced SINR condition does not hold for the problem with SIC ($\mathfrak{I}_k = \mathfrak{N}_k$) as described as follows.

Let us transform the problem (18) with $\mathfrak{I}_k = \mathfrak{N}_k$ to

$$\max_{\boldsymbol{p} \in \mathbb{R}_+^K} \ \gamma \tag{19a}$$

$$\text{subject to } \frac{p_k |\tilde{\boldsymbol{w}}_k^H \boldsymbol{h}_k|^2}{\sum\limits_{l=k+1}^{K} p_l |\tilde{\boldsymbol{w}}_k^H \boldsymbol{h}_l|^2 + \sigma^2 \|\tilde{\boldsymbol{w}}_k\|^2} \ge \gamma, \ \forall k \tag{19b}$$

$$p_k \le P_T |\boldsymbol{h}_k^T \tilde{\boldsymbol{v}}|^2, \ \forall k. \tag{19c}$$

The following lemmas describe some observations made on the optimal solution $\boldsymbol{p}^\dagger$ of (19):

Lemma 1: There exists at least one entry in $\boldsymbol{p}^\dagger$ that takes the maximum value in the individual power constraint of $p_k \le P_T|\boldsymbol{h}_k^T\tilde{\boldsymbol{v}}|^2$.

Proof: We use proof by contradiction herein. Assume that none of the optimal solution $\boldsymbol{p}^\dagger$ takes the maximum value in the individual power constraints in (19c) as $p_k^\dagger < P_T|\boldsymbol{h}_k^T\tilde{\boldsymbol{v}}|^2, \forall k$. We can then find a new solution $\boldsymbol{p}' = \zeta\boldsymbol{p}^\dagger$ with $\zeta = \min\limits_{1\le k\le K} \frac{P_T|\boldsymbol{h}_k^T\tilde{\boldsymbol{v}}|^2}{p_k^\dagger}$, where $\boldsymbol{p}'$ satisfies the individual power constraints in (19c) and leads to the following optimal value

$$\gamma_k|_{\boldsymbol{p}=\boldsymbol{p}'=\zeta\boldsymbol{p}^\dagger} = \frac{p_k^\dagger|\tilde{\boldsymbol{w}}_k^H\boldsymbol{h}_k|^2}{\sum\limits_{l=k+1}^{K} p_l^\dagger|\tilde{\boldsymbol{w}}_k^H\boldsymbol{h}_l|^2+\sigma^2\|\tilde{\boldsymbol{w}}_k\|^2/\zeta} \tag{20}$$

which is larger than $\gamma_k|_{\boldsymbol{p}=\boldsymbol{p}^\dagger}$ from $\zeta > 1$. Thus, at least one of BD should take the maximum value in the individual power constraint as $p_k^\dagger = P_T|\boldsymbol{h}_k^T\tilde{\boldsymbol{v}}|^2$. □

Lemma 2: Let k_o be the smallest index of BD that takes the maximum power as $p_{k_o}^\dagger = P_T|\boldsymbol{h}_{k_o}^T\tilde{\boldsymbol{v}}|^2$. For $\gamma_k^\dagger = \gamma_k|_{\boldsymbol{p}=\boldsymbol{p}^\dagger}$, the optimal value is given by $\gamma^\dagger = \gamma_{k_o}^\dagger$ with $\gamma_k^\dagger \ge \gamma^\dagger$ for $k < k_o$ and $\gamma_k^\dagger = \gamma^\dagger$ for $k > k_o$.

Proof: We first prove that $\gamma_k^\dagger = \gamma_{k_o}^\dagger$ for $k > k_o$ through proof by contradiction, where γ_k for $k > k_o$ depends only on p_k for $k > k_0$. Assume that $\gamma_k^\dagger > \gamma_{k_o}^\dagger$ for $k > k_o$. In this case, we can find another power allocation solution $p_k' < p_k^\dagger$ for $k > k_o$ that leads to $\gamma_k' < \gamma_k^\dagger$ for $k > k_o$ while increasing $\gamma_{k_o}' > \gamma_{k_o}^\dagger$, where γ_k' for $k > k_o$ denotes the SINR obtained with $p_{k_o}^\dagger$ and p_k' for $k > k_o$. It implies that a larger optimal value can be obtained with a new solution $\boldsymbol{p}' = [p_1^\dagger, \cdots, p_{k_o}^\dagger, p_{k_o+1}', \cdots, p_K']$, which violates that $\boldsymbol{p}^\dagger$ is the optimal solution. Thus, $\gamma_k^\dagger \le \gamma_{k_o}^\dagger$ for $k > k_o$. The optimal solution maximizing the minimum value makes $\gamma_k^\dagger = \gamma_{k_o}^\dagger$ for $k > k_o$.

We next prove that $\gamma_k^\dagger \ge \gamma_{k_o}^\dagger$ for $k < k_o$ via proof by contradiction again. Assume that $\gamma_k^\dagger < \gamma_{k_o}^\dagger$ for $k < k_o$. In this case, we can find another optimal solution $\boldsymbol{p}'$ with entry $p_k' = \zeta p_k^\dagger$ for $k < k_o$ and $p_k' = p_k^\dagger$ for $k \ge k_o$, where $\zeta = \min\limits_{1\le k<k_o} \frac{P_T|\boldsymbol{h}_k^T\tilde{\boldsymbol{v}}|^2}{p_k^\dagger}$; $\gamma_k' > \gamma_k^\dagger$ for $k < k_o$ so that $\min_{1\le k\le K}\gamma_k' > \min_{1\le k\le K}\gamma_k^\dagger$. In this case, k_o is not the minimum index of BD that takes the maximum value any more. This contradicts our assumption so that we should have $\gamma_k^\dagger \ge \gamma_{k_o}^\dagger$ for $k > k_o$. In addition, we can make $\gamma_k' > \gamma_{k_o}^\dagger$ for $k < k_o$ with another feasible solution $\boldsymbol{p}'$ with $p_k^\dagger < p_k' < P_T|\boldsymbol{h}_k^T\tilde{\boldsymbol{v}}|^2$ for $k < k_o$ and $p_k' = p_k^\dagger$ for $k \ge k_o$.[1]

Thus, the optimal value is given by $\gamma_{k_o}^\dagger$ with $\gamma_k^\dagger \ge \gamma_{k_o}^\dagger$ for $k < k_o$ and $\gamma_k^\dagger = \gamma_{k_o}^\dagger$ for $k \ge k_o$. □

[1]As a simple instance, we can increase p_1 up to its maximum value $P_T|\boldsymbol{h}_1^T\tilde{\boldsymbol{v}}|^2$ to make $\gamma_1 > \gamma_{k_o}^\dagger$ without changing the optimal value $\gamma_{k_o}^\dagger$

It is observed from the lemmas that the optimal solution $\boldsymbol{p}^\dagger$ of the power allocation problem (18) with SIC does not always balance the SINRs.

IV. PROPOSED ALTERNATING OPTIMIZATION ALGORITHM

This section presents a new algorithm to solve the original problem (13) or equivalently (14) without resorting to the balanced SINR condition. The proposed algorithm is also based on the alternating optimization of $\boldsymbol{W}$, $\boldsymbol{v}$, and $\boldsymbol{\beta}$ and is presented in a unified form for both cases of with and without SIC since it is also applicable to the problem without SIC.

A. RECEIVE BF OPTIMIZATION

For a given transmit BF $\boldsymbol{v} = \tilde{\boldsymbol{v}}$ and reflection coefficient $\boldsymbol{\beta} = \tilde{\boldsymbol{\beta}}$, the problem (14) becomes a receive BF optimization problem as

$$\max_{\boldsymbol{W}\in\mathbb{C}^{M\times K}} \left\{ \min_{1\le k\le K} \gamma_k \right\}, \tag{21}$$

where

$$\gamma_k = \frac{\tilde{p}_k|\boldsymbol{w}_k^H\boldsymbol{h}_k|^2}{\sum\limits_{l\in\mathfrak{I}_k} \tilde{p}_l|\boldsymbol{w}_k^H\boldsymbol{h}_l|^2 + \sigma^2\|\boldsymbol{w}_k\|^2} \tag{22}$$

with $\tilde{p}_k = P_T\tilde{\beta}_k|\boldsymbol{h}_k^T\tilde{\boldsymbol{v}}|^2$. Since γ_k depends only on $\boldsymbol{w}_k$ not on $\boldsymbol{w}_l$ for $l \ne k$, we have

$$\max_{\boldsymbol{W}\in\mathbb{C}^{M\times K}} \left\{ \min_{1\le k\le K} \gamma_k \right\} = \min_{1\le k\le K} \left\{ \max_{\boldsymbol{w}_k\in\mathbb{C}^M} \gamma_k \right\}, \tag{23}$$

which produces K independent optimization problems for the receive BF as

$$\max_{\boldsymbol{w}_k\in\mathbb{C}^M} \gamma_k, \ k = 1, 2, \cdots, K. \tag{24}$$

Each problem in (24) is a well-known Rayleigh quotient maximization problem [37] of which the optimal value is given by

$$\gamma_k^\dagger = p_k\boldsymbol{h}_k^H\boldsymbol{R}_k^{-1}\boldsymbol{h}_k \tag{25}$$

with $\boldsymbol{R}_k = \sum\limits_{l\in\mathfrak{I}_k} \tilde{p}_l\boldsymbol{h}_l\boldsymbol{h}_l^H + \sigma^2\boldsymbol{I}_M$. The optimal receive BF achieving the optimal value is given as

$$\boldsymbol{w}_k^\dagger = c_k\boldsymbol{R}_k^{-1}\boldsymbol{h}_k, \tag{26}$$

where c_k is any nonzero constant that can be ignored.

The computation of the optimal receive BF can be facilitated from the following facts: The optimal receive BF without SIC ($\mathfrak{I}_k = \mathfrak{O}_k$) is equivalent to the minimum mean square error (MMSE) receive BF as

$$\boldsymbol{w}_k^\dagger = (\boldsymbol{H}\tilde{\boldsymbol{P}}\boldsymbol{H}^H + \sigma^2\boldsymbol{I}_M)^{-1}\boldsymbol{h}_k, \tag{27}$$

where $\boldsymbol{H} = [\boldsymbol{h}_1, \boldsymbol{h}_2, \cdots, \boldsymbol{h}_K]$ and $\tilde{\boldsymbol{P}} = \mathrm{diag}([\tilde{p}_1, \tilde{p}_2, \cdots, \tilde{p}_K])$. The optimal receive BF with SIC ($\mathfrak{I}_k = \mathfrak{N}_k$) can be computed sequentially from $k = K-1$ to 1 with $\boldsymbol{w}_K^\dagger = \boldsymbol{h}_K$ as

$$\boldsymbol{w}_k^\dagger = \boldsymbol{R}_k^{-1}\boldsymbol{h}_k = \boldsymbol{R}_{k+1}^{-1}\boldsymbol{h}_k - \frac{\boldsymbol{w}_{k+1}^\dagger(\boldsymbol{w}_{k+1}^\dagger)^H\boldsymbol{h}_k}{1+\boldsymbol{h}_{k+1}^H\boldsymbol{w}_{k+1}^\dagger} \tag{28}$$

from the Sherman–Morrison formula resulting in

$$\boldsymbol{R}_k^{-1} = \boldsymbol{R}_{k+1}^{-1} - \frac{\boldsymbol{R}_{k+1}^{-1}\boldsymbol{h}_{k+1}\boldsymbol{h}_{k+1}^H\boldsymbol{R}_{k+1}^{-1}}{1+\boldsymbol{h}_{k+1}^H\boldsymbol{R}_{k+1}^{-1}\boldsymbol{h}_{k+1}} \tag{29}$$

for $k = 1, 2, \cdots, K-1$ with $\boldsymbol{R}_K = \sigma^2\boldsymbol{I}_M$.

B. TRANSMIT BF OPTIMIZATION

For a given receive BF $\boldsymbol{W} = \tilde{\boldsymbol{W}}$ and reflection coefficient $\boldsymbol{\beta} = \tilde{\boldsymbol{\beta}}$, the problem (14) becomes the transmit BF optimization problem as follows:

$$\max_{\boldsymbol{v}\in\mathbb{C}^M:\|\boldsymbol{v}\|^2\le 1}\left\{\min_{1\le k\le K}\gamma_k(\boldsymbol{v})\right\}, \tag{30}$$

where

$$\gamma_k(\boldsymbol{v}) = \frac{a_{k,k}|\boldsymbol{h}_k^T\boldsymbol{v}|^2}{\sum\limits_{l\in\mathfrak{I}_k} a_{k,l}|\boldsymbol{h}_l^T\boldsymbol{v}|^2 + b_k} \tag{31}$$

with $a_{k,l} = P_T\tilde{\beta}_l|\tilde{\boldsymbol{w}}_k^H\boldsymbol{h}_l|^2$ and $b_k = \sigma^2\|\tilde{\boldsymbol{w}}_k\|^2$. The problem (30) is equivalent to

$$\max_{\boldsymbol{v}\in\mathbb{C}^M:\|\boldsymbol{v}\|^2\le 1, t\in\mathbb{R}_+} \quad t \tag{32a}$$

$$\text{subject to} \quad \gamma_k(\boldsymbol{v}) \ge t \ \forall k, \tag{32b}$$

where the nonconvexity of (32b) with respect to $\boldsymbol{v}$ makes the problem difficult to solve.

To handle the nonconvex constraints (32b), we apply a successive convex approximation (SCA) method [45] using the first-order Taylor series approximation $\hat{\gamma}_k(\boldsymbol{v}, \boldsymbol{v}_\diamond)$ of (31) around a feasible vector $\boldsymbol{v}_\diamond$. The approximation is derived in the Appendix as follows:

$$\hat{\gamma}_k(\boldsymbol{v}, \boldsymbol{v}_\diamond) = \gamma_k(\boldsymbol{v}_\diamond) + \frac{\gamma_k(\boldsymbol{v}_\diamond)}{\rho_k(\boldsymbol{v}_\diamond)}L_k(\boldsymbol{v}, \boldsymbol{v}_\diamond), \tag{33}$$

where $\rho_k(\boldsymbol{v}) = |\boldsymbol{h}_k^T\boldsymbol{v}|^2$ and

$$L_k(\boldsymbol{v}, \boldsymbol{v}_\diamond) = \tilde{\rho}_k(\boldsymbol{v}, \boldsymbol{v}_\diamond) - \frac{\gamma_k(\boldsymbol{v}_0)}{a_{k,k}}\sum_{l=k+1}^{K} a_{k,l}\tilde{\rho}_l(\boldsymbol{v}, \boldsymbol{v}_\diamond) \tag{34}$$

with

$$\tilde{\rho}_l(\boldsymbol{v}, \boldsymbol{v}_\diamond) = 2\Re\{\boldsymbol{v}_\diamond^H\boldsymbol{h}_l^*\boldsymbol{h}_l^T(\boldsymbol{v}-\boldsymbol{v}_\diamond)\}. \tag{35}$$

It should be also noted that $\tilde{\rho}_l(\boldsymbol{v}, \boldsymbol{v}_\diamond) = \hat{\rho}_l(\boldsymbol{v}, \boldsymbol{v}_\diamond) - \rho_l(\boldsymbol{v}_\diamond)$, where $\hat{\rho}_l(\boldsymbol{v}, \boldsymbol{v}_\diamond)$ is the first-order Taylor series approximation of $\rho_l(\boldsymbol{v})$ around $\boldsymbol{v}_\diamond$.

An approximate problem of (32) is then expressed as

$$\max_{\boldsymbol{v}\in\mathbb{C}^M:\|\boldsymbol{v}\|^2\le 1, \tilde{t}\in\mathbb{R}_+} \quad \tilde{t} \tag{36a}$$

$$\text{subject to} \quad \hat{\gamma}_k(\boldsymbol{v}, \boldsymbol{v}_\diamond) \ge \tilde{t}, \ \forall k, \tag{36b}$$

which is a quadratically constrained linear program (QCLP) [46]. The solution of (32) is found by solving (36) in an iterative way by setting $\boldsymbol{v}_\diamond$ at the lth iteration to $\boldsymbol{v}_l^\star$, where $(\boldsymbol{v}_m^\star, \tilde{t}_m^\star)$ is the solution of (36) at the mth iteration.

C. REFLECTION COEFFICIENT OPTIMIZATION

For a given receive BF $\boldsymbol{W} = \tilde{\boldsymbol{W}}$ and transmit BF $\boldsymbol{v} = \tilde{\boldsymbol{v}}$, (14) becomes the reflection coefficient optimization problem as

$$\max_{0\le\boldsymbol{\beta}\le 1}\left\{\min_{1\le k\le K}\ \gamma_k \triangleq \frac{\phi_{k,k}\beta_k}{\sum_{l\in\mathfrak{I}_k}\phi_{k,l}\beta_l + b_k}\right\}, \tag{37}$$

where

$$\phi_{k,l} = P_T|\tilde{\boldsymbol{w}}_k^H\boldsymbol{h}_l|^2|\boldsymbol{h}_l^T\tilde{\boldsymbol{v}}|^2. \tag{38}$$

We transform (37) into

$$\max_{\boldsymbol{\beta}\in[0,1]^K, \gamma\in\mathbb{R}_+} \quad \gamma \tag{39a}$$

$$\text{subject to} \quad \left(\boldsymbol{\Phi} - \tfrac{1}{\gamma}\boldsymbol{I}_K\right)\boldsymbol{\beta} + \boldsymbol{q} \le 0, \tag{39b}$$

where $\boldsymbol{q} = [\frac{b_1}{\phi_{1,1}}, \frac{b_2}{\phi_{2,2}}, \cdots, \frac{b_K}{\phi_{K,K}}]^T$ and $\boldsymbol{\Phi}$ is constructed by the (k,l)th entry given below:

$$\Phi_{k,l} = \begin{cases} \dfrac{\phi_{k,l}}{\phi_{k,k}} & \text{if } l \in \mathfrak{I}_k \\ 0 & \text{otherwise.} \end{cases} \tag{40}$$

That is, the nonzero elements of $\boldsymbol{\Phi}$ are given for $l > k$ with SIC ($\mathfrak{I}_k = \mathfrak{N}_k$) and for $l \ne k$ without SIC ($\mathfrak{I}_k = \mathfrak{O}_k$). We find the optimal solution γ^+ and $\boldsymbol{\beta}^+$ of the problem (39) by finding the maximum γ of leading a feasible solutions in the linear programming feasibility (LPF) problem for given γ through a bisection search [46].

For the problem with SIC, we find the new reflection coefficient vector $\boldsymbol{\beta}^\ddagger$ from the optimal solution $\boldsymbol{\beta}^+$ found with the LPF problems to maximize the harvested energy at the BDs without changing the max–min SINR γ^+. Based on Lemma 2, we have $\beta_k^\ddagger = \beta_k^+$ for $k \ge k_o$ with the minimum index k_o of the BD resulting the max–min SINR γ^+, and obtain $\beta_k^\ddagger$ for $k < k_0$ sequentially as

$$\beta_k^\ddagger = \gamma^+\left(\sum_{l=k+1}^{K}\Phi_{k,l}\beta_l^\ddagger + q_k\right) \tag{41}$$

from $k = k_o - 1$ to 1. This adjustment reduces the reflected portion at the BDs operating at a higher SINR than the max–min SINR to increase the energy harvested from the unreflected signals. The optimal reflection coefficient for the problem without SIC remain unchanged as $\boldsymbol{\beta}^\ddagger = \boldsymbol{\beta}^+$.

D. OVERALL ALGORITHM

The proposed algorithm finding the solution of (14) is summarized in Algorithm 1. Initially, we set the transmit BF to be isotropic as $\boldsymbol{v}^{(0)} = \frac{1}{\sqrt{M}}\boldsymbol{1}_K$ and reflection coefficient to be maximum as $\boldsymbol{\beta}^{(0)} = \boldsymbol{1}_K$. We optimize the receive BF and then optimize the transmit BF via SCA with the updated receive BF until the SCA iteration reaches its maximum value $I_{\max}^{sca}$ or the optimal value is converged within a tolerance error ϵ, and we then optimize the reflection coefficients. This process continues until the outer iteration reaches its maximum value $I_{\max}^{out}$ or the optimal value is converged within a tolerance

Algorithm 1 Proposed Alternating Optimization Algorithm

Initialize: Set $n \leftarrow 0$, $\boldsymbol{v}^{(0)} \leftarrow \frac{1}{\sqrt{M}}\mathbf{1}_K$, and $\boldsymbol{\beta}^{(0)} \leftarrow \mathbf{1}_K$.
repeat
  $n \leftarrow n+1$.
  Receive BF: Compute (26) for $\boldsymbol{W}^{(n)}$ with $\tilde{\boldsymbol{v}} = \boldsymbol{v}^{(n-1)}$ and $\tilde{\boldsymbol{\beta}} = \boldsymbol{\beta}^{(n-1)}$.
  Transmit BF: Set $l \leftarrow 0$, $\tilde{\boldsymbol{W}} \leftarrow \boldsymbol{W}^{(n)}$, $\tilde{\boldsymbol{\beta}} \leftarrow \boldsymbol{\beta}^{(n-1)}$, and $\boldsymbol{v}_\diamond \leftarrow \boldsymbol{v}^{(n-1)}$.
  repeat
    $l \leftarrow l+1$.
    Solve (36) to find the optimal solution $(\boldsymbol{v}_l^\star, \tilde{t}_l^\star)$.
    $\boldsymbol{v}_\diamond \leftarrow \boldsymbol{v}_l^\star$.
  until $l \le I_{\max}^{sca}$ and $|\tilde{t}_l^\star - \tilde{t}_{l-1}^\star| < \epsilon$.
  Set $\boldsymbol{v}^{(n)} \leftarrow \boldsymbol{v}_l^\star$.
  Reflection coefficient : Solve (39) with $\tilde{\boldsymbol{W}} = \boldsymbol{W}^{(n)}$ and $\tilde{\boldsymbol{v}} = \boldsymbol{v}^{(n)}$ to obtain $(\gamma^{(n)}, \boldsymbol{\beta}^{(n)})$.
  if SIC is enabled **then**
    Update $\boldsymbol{\beta}^{(n)}$ with (41).
  end if
until $n \le I_{\max}^{out}$ or $|\gamma^{(n)} - \gamma^{(n-1)}| < \epsilon$.
Output: $(\hat{\gamma}^o, \hat{\boldsymbol{W}}^o, \hat{\boldsymbol{v}}^o, \hat{\boldsymbol{\beta}}^o) \leftarrow (\gamma^{(n)}, \boldsymbol{W}^{(n)}, \boldsymbol{v}^{(n)}, \boldsymbol{\beta}^{(n)})$.

error ϵ. The algorithm outputs approximate optimal variables $(\hat{\boldsymbol{W}}^o, \hat{\boldsymbol{v}}^o, \hat{\boldsymbol{\beta}}^o)$ and value $\hat{\gamma}_o$ with which the max–min rate is computed as $\hat{R}_{\min}^o = \log_2(1+\hat{\gamma}_o)$.

E. DISCUSSIONS

The proposed algorithm provides a different approach in the transmit BF and reflection coefficient optimization when compared with the existing SRM-based algorithm designed for SDMA without SIC [44]. The transmit BF optimization in the proposed algorithm requires a complexity of $O(8I_{\max}^{\text{sca}}M^3)$ by solving the QCLP problem with M complex variables (of complexity $O(8M^3)$ using an interior-point method [45]) up to $I_{\max}^{\text{sca}}$ times. The reflection coefficient optimization in the proposed method is solved at $O(\lceil\log_2\frac{1}{\epsilon}\rceil K^3)$ through a bisection search of the optimal value with LPF problems with K variables. On the other hand, the conventional algorithm in [44] requires $O((2M^2+K+2)^3)$ in solving a general convex problem with M^2 complex variables and $K+2$ real variables to find the transmit BF and reflection coefficient jointly. Thus, the proposed algorithm with a reasonable choice of $I_{\max}^{\text{sca}}$ and ϵ can be applied to the case without SIC to lower the computational complexity of the conventional algorithm. It should be also mentioned that all the computational burden of finding the solution of the proposed algorithm is imposed to the reader.

The channel state information (CSI) $\{\boldsymbol{h}_k\}_{k=1}^K$ required at the reader for the proposed algorithm can be obtained by applying the channel estimation (CE) methods proposed in [12], [17], which allocate a CE phase before a data transmission phase in a frame. The reader transmits orthogonal training signals in K time slots of the CE phase so that BD D_k assigned to the kth time slot reflects the signal with a known reflection coefficient. From that reflected signal from BD D_k, the reader estimates the CSI $\boldsymbol{h}_k$ by exploiting the channel reciprocity as in [17]. This approach relocates the complexity and energy consumption from the BDs to the reader so that the energy consumption of the BDs in the CSI acquisition is negligible although a rate loss is incurred by the additional CE phase. After finding the solution of the proposed algorithm, the reader broadcasts the reflection coefficients to the BDs over a control channel that is positioned between the CE and data transmission phases. This control channel also leads to an additional rate loss but the loss is relatively small in general for a large amount of the uplink data.

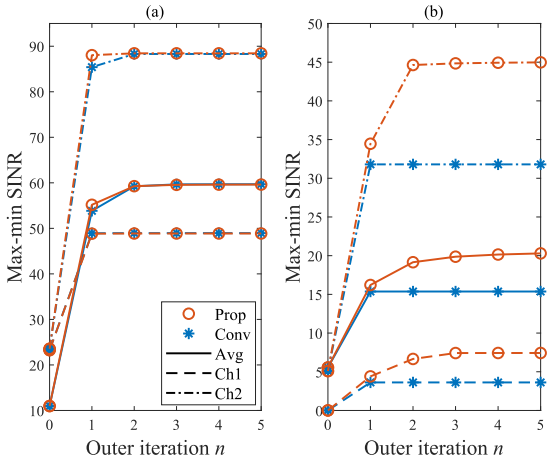

FIGURE 2. Convergence behaviors of the alternating algorithms as the outer iteration increases when $P_T = 30$ dBm and $M = 4$; (a) $K = 4$ without SIC and (b) $K = 8$ with SIC.

In addition, the solution of the proposed algorithm obtained with the estimated CSI causes a performance degradation as observed in any other practical systems. Nonetheless, the proposed algorithm can still provide a gain over an unoptimized system if the channel estimation error is not so large. In the meantime, for a more robust performance with imperfect CSI and SIC, the optimization problem in this paper can be extended to a robust beamforming design problem studied for the SWIPT systems in [42], [43]. Such performance investigations and robust beamforming designs with the imperfect CSI and SIC would be interesting subjects which are beyond the scope of this paper and are reserved for a future study.

V. SIMULATION RESULTS

We evaluate the performance of the monostatic MBCN when BDs are located in an annular region of inner radius 2 m and outer radius 10 m. The path loss is given by $\omega_k = 0.001 d_k^{-2.5}$ and the noise power is set to $\sigma^2 = -90$ dBm. The SIC is performed in the order of channel power to have $\|\boldsymbol{h}_1\| > \|\boldsymbol{h}_2\| > \cdots > \|\boldsymbol{h}_K\|$ as in [34], [35], [37]. The average performance is evaluated with 10^3 channel realizations, where the locations of BDs are chosen randomly in the aforementioned region for each channel realization.

To begin with, we provide some convergence behaviors of the proposed and conventional [44] alternating algorithms in Fig. 2 when $P_T = 30$ dBm and $M = 4$. The max–min

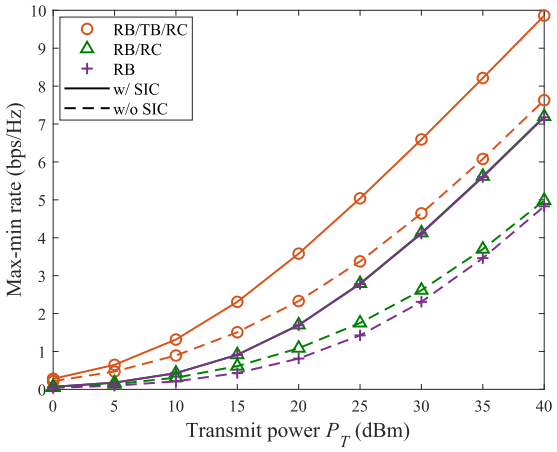

FIGURE 3. Average max–min rate of the SDMA as the transmit power P_T increases when $M = 4$ and $K = 4$.

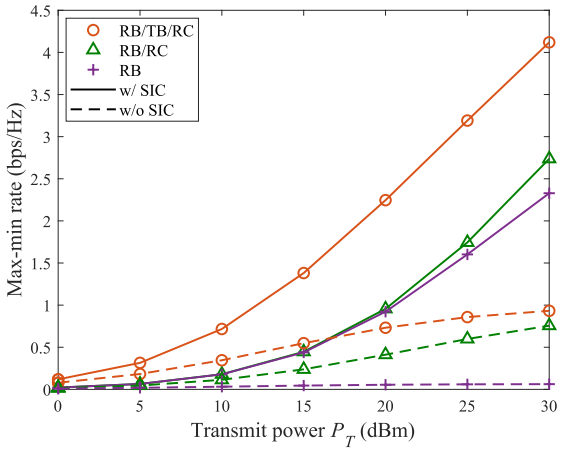

FIGURE 4. Average max–min rate of the NOMA/SDMA as the transmit power P_T increases when $M = 4$ and $K = 8$.

SINR $\gamma^{(n)}$ is shown as a function of the outer iteration n when a tolerance error is set to $\epsilon = 10^{-3}$ in the iterative processes required for the proposed (''Prop'') and conventional (''Conv'') algorithms with $I_{\max}^{\text{sca}} = 5$ for the proposed algorithm. Figure 2(a) represents an SDMA case with $K = 4$ having no SIC, and Fig. 2(b) represents a NOMA/SDMA case with $K = 8$ employing SIC. In the figures, ''Ch1'' and ''Ch2'' represent the results of two single-channel realizations chosen randomly for each subfigure and ''Average'' denotes the results averaged by 10^3 channel realizations for each subfigure. Both algorithms show a convergence for $n > 3$ in most of channel realizations and in average although the results for only two channel realizations are shown to avoid crowded graphs. The proposed algorithm provides a similar performance with the conventional one in Fig. 2(a) representing SDMA without SIC while the former outperforms the latter significantly in Fig. 2(b) representing NOMA/SDMA with SIC. The figures confirm that the proposed algorithm can be applied whether the balanced SINR condition is satisfied or not. Thus, we set $I_{\max}^{\text{out}} = 5$ for the proposed and conventional algorithms and use the proposed algorithm for most of performance comparisons in the following sections.

The average max–min rate of the MBCN with different optimization variables is compared as a function of the transmit power P_T in Fig. 3 when $M = 4$ and $K = 4$ for SDMA and in Fig. 4 when $M = 4$ and $K = 8$ for NOMA/SDMA. In the figures, RB/TB/RC denotes the proposed algorithm optimizing the transmit BF, receive BF, and reflection coefficients while RB/RC optimizes the receive BF and reflection coefficients with $\boldsymbol{v} = \frac{1}{M}\mathbf{1}_M$ as in [37], and RB optimizes the receive BF with $\boldsymbol{v} = \frac{1}{M}\mathbf{1}_M$ and $\boldsymbol{\beta} = \mathbf{1}_K$. The algorithms are applied for the problem with SIC and that without SIC, respectively, in both figures. It is obvious that the performance is the best in the order of TB/RB/RC, RB/RC, and RB. The gain of RB/TB/RC over RB/RC is more pronounced than that of RB/RC over RB in Fig. 3 for SDMA with and without SIC and in Fig. 4 with SIC. This observation confirms that the transmit BF optimization leverages the overall optimization performance significantly. The figures also confirm that SDMA is implementable without and with SIC in Fig. 3 while NOMA/SDMA is not viable without SIC as observed in in Fig. 4. The gain attained by employing SIC in SDMA is not as huge as that in NOMA/SDMA, but the gain is not negligible in particular as the transmit power increases.

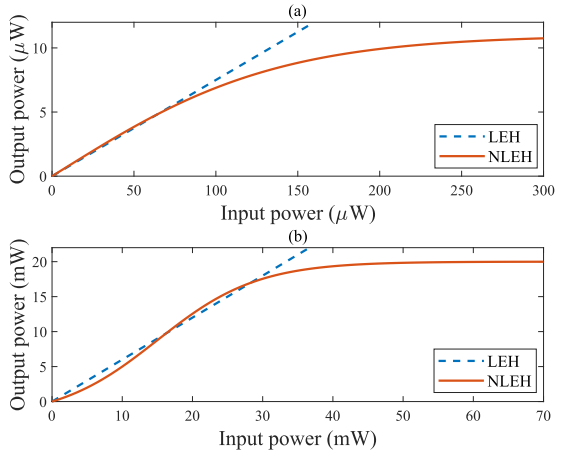

FIGURE 5. Two EH models employed in performance evaluation: (a) EH model I (b) EH model II.

In the meantime, the average total harvested energy given by

$$\mathbb{E}[E_{\text{total}}] = \sum_{k=1}^{K} \mathbb{E}[E_k] \tag{42}$$

is obtained by using the EH models in Fig 5 similar to the those in [5] during the simulations for Figs. 3 and 4. The NLEH function in Fig. 5(a) for EH model I is obtained with $P_{\text{sat}} = 11$ μW, $a = 15000$, and $p_c = 5$ μW in (4) and is approximated by the LEH function (3) with $\eta_{\text{eff}} = 0.075$ whilst the NLEH function in Fig. 5(b) for EH model II is obtained with $P_{\text{sat}} = 20$ mW, $a = 140$, and $p_c = 15$ mW and is approximated by the LEH function with $\eta_{\text{eff}} = 0.6$. Figs. 6 and 7 provide the average total harvested energy of the system with SIC by using the EH models of Figs. 5(a) and 5(b), respectively; The left subfigures are obtained with $M = 4$ and $K = 4$ and the right ones are obtained with $M = 4$ and $K = 8$, where ''RB'' leading to the zero energy

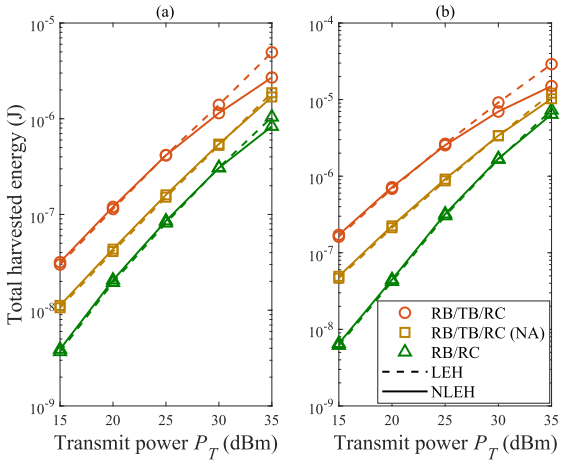

FIGURE 6. Average harvested energy in the network with EH model I as the transmit power P_T increases: (a) $M = 4$ and $K = 4$ (b) $M = 4$ and $K = 8$.

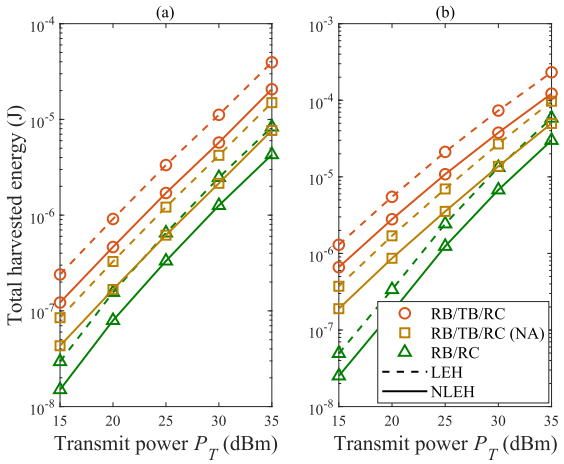

FIGURE 7. Average harvested energy in the network with EH model II as the transmit power P_T increases: (a) $M = 4$ and $K = 4$ (b) $M = 4$ and $K = 8$.

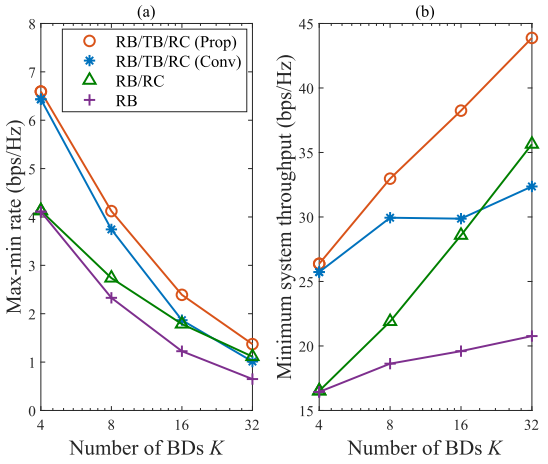

FIGURE 8. Average max–min rate and minimum system throughput with SIC as the number K of BDs increases when $M = 4$ and $P_T = 30$ dBm.

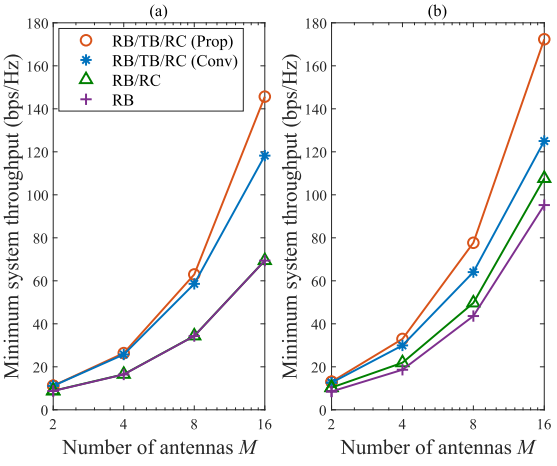

FIGURE 9. Average max-min rate of the system with SIC as a function of the number M of antennas when $P_T = 30$ dBm: (a) SDMA with $K = M$ (b) NOMA/SDMA with $K = 2M$.

due to full reflection is not shown and "RB/TB/RC (NA)" representing the proposed algorithm without (41) is shown instead. The total harvested energy in the network is improved by employing the reflection coefficient adjustment (41) of the proposed algorithm for both EH models. Fig. 6 shows that the harvested energy with the NLEH function of model I is saturated at a high transmit power P_T since its saturation power is as small as $P_{\text{sat}} = 11$ μW. The total harvested energy with the NLEH function of model II is not saturated but is smaller than that with the LEH approximation since the input to the NLEH function tends to be in a convex region of the sigmoid-like function. It is also observed that the total harvested energy increases as the number of BDs increases from $K = 4$ to 8 since the common excitation signal can be shared for energy harvesting by more BDs. The transmit BF optimization also increases the total harvested energy with a larger gain for a larger number of BDs.

Figure 8 compares the performance of the MBCN with SIC as the number K of BDs increases while fixing $M = 4$ and $P_T = 30$ dBm. The left subfigure provides the average max–min rate $\mathbb{E}[\hat{R}^o_{\min}]$, and the right subfigure provides the minimum system throughput $\mathbb{E}[KR^o_{\min}]$ provided by the network. In the figure, we also compare the performance of the proposed algorithm denoted by "TB/RB/RC (Prop)" and the conventional algorithm [44] denoted by "TB/RB/RC (Conv)" for the joint optimization. Although the average max–min rate decreases as the number K of BDs increases in Fig. 8(a) to guarantee the fairness of more BDs, the minimum system throughput increases with K in Fig. 8(b) by allowing more devices. As the number of BDs increases, the benefit of reflection coefficient optimization also increases, that is, the gain of RB/RC over RB gets larger, since the number K of variables in the reflection coefficient optimization also increases. The gain of RB/TB/RC over RB/RC in the minimum system throughput remains unchanged for K in Fig. 8(b) since the optimizing variables in the transmit BF are unchanged by fixing $M = 4$. It is also observed that the conventional algorithm provides a

significant loss compared with the proposed algorithm and the loss gets larger as the number of BDs increases.

We also compare the minimum system throughput of the MBCN with SIC in Fig. 9 as the number M of antennas increases for SDMA with $K = M$ in Fig. 9(a) and for NOMA/SDMA with $K = 2M$ in Fig. 9(b). In both figures, we set the transmit power as $P_T = 30$ dBm. Again, the proposed algorithm provides a significant gain over the algorithms without transmit BF optimization (RB/RC and RB) and the gain increases with the number of antennas. Although the conventional algorithm exhibits a better performance than RB/RC and RB, it cannot compete with the proposed algorithm in particular for a large number of antennas and a large number of devices. The two subfigures also imply that NOMA/SDMA provides a larger minimum system throughput than SDMA for a given number of antennas.

VI. CONCLUSION

This article considered a monostatic BackCom network with a multiantenna reader and multiple BDs served by SDMA or NOMA/SDMA simultaneously. The full-duplex reader transmits an excitation signal with the transmit BF and receives the backscatter signals from the BDs with the receive BF and SIC, where the BDs reflect their incident signals with different reflection coefficients for the information transfer to the reader. We formulated a joint optimization problem of the receive BF, transmit BF, and reflection coefficients toward the maximum fairness for the network with and without SIC. The problem without SIC was shown to be equivalent to a joint optimization problem solved for a WPCN based on the balanced SINR condition. After showing that the problem with SIC does not satisfy the balanced SINR condition always, we proposed a new alternating optimization algorithm that is applicable to the problem with and without SIC at a reduced complexity. We confirmed the validity and merits of the proposed algorithm through simulations. We first showed that the proposed algorithm provides a similar performance with the conventional joint optimization algorithm for the problem without SIC to justify the proposed algorithm. We then showed an outstanding gain of the proposed algorithm over the conventional ones in solving the problem with SIC. In particular, the transmit BF optimization added in the proposed algorithm can improve the rate fairness as well as the sum energy harvested in the network. In addition, it was shown that NOMA/SDMA with SIC can increase the minimum system throughput significantly by accepting more BDs for a given number of antennas. From the results, the proposed algorithm has also shown promising applications to WPCN employing a similar multiple access scheme considered herein.

TAYLOR SERIES APPROXIMATION OF THE SINR

The first-order Taylor series approximation of (31) with respect to $\boldsymbol{v} = [v_1, v_2, \cdots, v_M]^T$ is expressed below.

$$\hat{\gamma}_k(\boldsymbol{v}, \boldsymbol{v}_\diamond) = \gamma_k(\boldsymbol{v}_\diamond) + 2\Re\left\{[\nabla_{\boldsymbol{v}^*}\gamma_k(\boldsymbol{v}_\diamond)]^H(\boldsymbol{v} - \boldsymbol{v}_\diamond)\right\} \tag{43}$$

where $\nabla_{\boldsymbol{v}^*}\gamma_k(\boldsymbol{v}) = [\frac{\partial\gamma_k}{\partial v_1^*}, \frac{\partial\gamma_k}{\partial v_2^*}, \cdots \frac{\partial\gamma_k}{\partial v_M^*}]^T$. Let us rewrite $\gamma_k(\boldsymbol{v})$ as

$$\gamma_k(\boldsymbol{v}) = \frac{a_{k,k}\rho_k(\boldsymbol{v})}{D_k(\boldsymbol{v})} \tag{44}$$

with

$$\rho_k(\boldsymbol{v}) = \boldsymbol{v}^H\boldsymbol{h}_k^*\boldsymbol{h}_k^T\boldsymbol{v} \tag{45}$$

and $D_k(\boldsymbol{v}) = \sum_{l\in\mathfrak{I}_k} a_{k,l}\rho_l(\boldsymbol{v}) + b_k$. We then obtain

$$\begin{aligned}\nabla_{\boldsymbol{v}^*}\gamma_k(\boldsymbol{v}) &= \frac{a_{k,k}}{D_k(\boldsymbol{v})}\boldsymbol{h}_k^*\boldsymbol{h}_k^T\boldsymbol{v} - \frac{a_{k,k}\rho_k(\boldsymbol{v})}{D_k^2(\boldsymbol{v})}\sum_{l\in\mathfrak{I}_k} a_{k,l}\boldsymbol{h}_l^*\boldsymbol{h}_l^T\boldsymbol{v} \\ &= \frac{\gamma_k(\boldsymbol{v})}{\rho_k(\boldsymbol{v})}\boldsymbol{h}_k^*\boldsymbol{h}_k^T\boldsymbol{v} - \frac{\gamma_k^2(\boldsymbol{v})}{a_{k,k}\rho_k(\boldsymbol{v})}\sum_{l\in\mathfrak{I}_k} a_{k,l}\boldsymbol{h}_l^*\boldsymbol{h}_l^T\boldsymbol{v}\end{aligned} \tag{46}$$

from $\nabla_{\boldsymbol{v}^*}\rho_k(\boldsymbol{v}) = \boldsymbol{h}_k^*\boldsymbol{h}_k^T\boldsymbol{v}$ and $\nabla_{\boldsymbol{v}^*}D_k(\boldsymbol{v}) = \sum_{l\in\mathfrak{I}_k} a_{k,l}\boldsymbol{h}_l^*\boldsymbol{h}_l^T\boldsymbol{v}$. We then substitute (46) with $\boldsymbol{v} = \boldsymbol{v}_\diamond$ into (43) to get the equation

$$\begin{aligned}\hat{\gamma}_k(\boldsymbol{v}, \boldsymbol{v}_\diamond) = \gamma_k(\boldsymbol{v}_\diamond) &+ 2\frac{\gamma_k(\boldsymbol{v}_\diamond)}{\rho_k(\boldsymbol{v}_\diamond)}\Re\{\boldsymbol{v}_\diamond^H\boldsymbol{h}_k^*\boldsymbol{h}_k^T(\boldsymbol{v} - \boldsymbol{v}_\diamond)\} \\ &- 2\frac{\gamma_k^2(\boldsymbol{v}_\diamond)}{a_{k,k}\rho_k(\boldsymbol{v}_\diamond)}\sum_{l\in\mathfrak{I}_k} a_{k,l}\Re\{\boldsymbol{v}_\diamond^H\boldsymbol{h}_l^*\boldsymbol{h}_l^T(\boldsymbol{v} - \boldsymbol{v}_\diamond)\}\end{aligned} \tag{47}$$

which becomes (33) with $L_k(\boldsymbol{v}, \boldsymbol{v}_\diamond)$ and $\tilde{\rho}_l(\boldsymbol{v}, \boldsymbol{v}_\diamond)$ defined in (34) and (35), respectively.

REFERENCES

[1] M. Giordani, M. Polese, M. Mezzavilla, S. Rangan, and M. Zorzi, "Toward 6G networks: Use cases and technologies," *IEEE Commun. Mag.*, vol. 58, no. 3, pp. 55–61, Mar. 2020.

[2] W. Saad, M. Bennis, and M. Chen, "A vision of 6G wireless systems: Applications, trends, technologies, and open research problems," *IEEE Netw.*, vol. 34, no. 3, pp. 134–142, May 2020.

[3] Q. Shi, L. Liu, W. Xu, and R. Zhang, "Joint transmit beamforming and receive power splitting for MISO SWIPT systems," *IEEE Trans. Wireless Commun.*, vol. 13, no. 6, pp. 3269–3280, Jun. 2014.

[4] D. W. K. Ng, E. S. Lo, and R. Schober, "Robust beamforming for secure communication in systems with wireless information and power transfer," *IEEE Trans. Wireless Commun.*, vol. 13, no. 8, pp. 4599–4615, Aug. 2014.

[5] E. Boshkovska, D. W. K. Ng, N. Zlatanov, and R. Schober, "Practical non-linear energy harvesting model and resource allocation for SWIPT systems," *IEEE Commun. Lett.*, vol. 19, no. 12, pp. 2082–2085, Dec. 2015.

[6] S. Bi, Y. Zeng, and R. Zhang, "Wireless powered communication networks: An overview," *IEEE Wireless Commun.*, vol. 23, no. 2, pp. 10–18, Apr. 2016.

[7] D. Niyato, D. I. Kim, M. Maso, and Z. Han, "Wireless powered communication networks: Research directions and technological approaches," *IEEE Wireless Commun.*, vol. 24, no. 6, pp. 88–97, Dec. 2017.

[8] C. Boyer and S. Roy, "Coded QAM backscatter modulation for RFID," *IEEE Trans. Commun.*, vol. 60, no. 7, pp. 1925–1934, Jul. 2012.

[9] C. Boyer and S. Roy, "Backscatter communication and RFID: Coding, energy, and MIMO analysis," *IEEE Trans. Commun.*, vol. 62, no. 3, pp. 770–785, Mar. 2014.

[10] C. Xu, L. Yang, and P. Zhang, "Practical backscatter communication systems for battery-free Internet of Things: A tutorial and survey of recent research," *IEEE Signal Process. Mag.*, vol. 35, no. 5, pp. 16–27, Sep. 2018.

[11] N. Van Huynh, D. T. Hoang, X. Lu, D. Niyato, P. Wang, and D. I. Kim, "Ambient backscatter communications: A contemporary survey," *IEEE Commun. Surveys Tuts.*, vol. 20, no. 4, pp. 2889–2922, 4th Quart., 2018.

[12] G. Yang, C. K. Ho, and Y. L. Guan, "Multi-antenna wireless energy transfer for backscatter communication systems," *IEEE J. Sel. Areas Commun.*, vol. 33, no. 12, pp. 2974–2987, Dec. 2015.

[13] B. Clerckx, Z. B. Zawawi, and K. Huang, "Wirelessly powered backscatter communications: Waveform design and SNR-energy tradeoff," *IEEE Commun. Lett.*, vol. 21, no. 10, pp. 2234–2237, Oct. 2017.

[14] I. Krikidis, "Retrodirective large antenna energy beamforming in backscatter multi-user networks," *IEEE Wireless Commun. Lett.*, vol. 7, no. 4, pp. 678–681, Aug. 2018.
[15] J. C. Kwan and A. O. Fapojuwo, "Sum-throughput maximization in wireless sensor networks with radio frequency energy harvesting and backscatter communication," *IEEE Sensors J.*, vol. 18, no. 17, pp. 7325–7339, Sep. 2018.
[16] Z. B. Zawawi, Y. Huang, and B. Clerckx, "Multiuser wirelessly powered backscatter communications: Nonlinearity, waveform design, and SINR-energy tradeoff," *IEEE Trans. Wireless Commun.*, vol. 18, no. 1, pp. 241–253, Jan. 2019.
[17] D. Mishra and E. G. Larsson, "Optimal channel estimation for reciprocity-based backscattering with a full-duplex MIMO reader," *IEEE Trans. Signal Process.*, vol. 67, no. 6, pp. 1662–1677, Mar. 2019.
[18] D. Mishra and E. G. Larsson, "Sum throughput maximization in multi-tag backscattering to multiantenna reader," *IEEE Trans. Commun.*, vol. 67, no. 8, pp. 5689–5705, Aug. 2019.
[19] D. Mishra and E. G. Larsson, "Multi-tag backscattering to MIMO reader: Channel estimation and throughput fairness," *IEEE Trans. Wireless Commun.*, vol. 18, no. 12, pp. 5584–5599, Dec. 2019.
[20] K. Han and K. Huang, "Wirelessly powered backscatter communication networks: Modeling, coverage, and capacity," *IEEE Trans. Wireless Commun.*, vol. 16, no. 4, pp. 2548–2561, Apr. 2017.
[21] G. Wang, F. Gao, R. Fan, and C. Tellambura, "Ambient backscatter communication systems: Detection and performance analysis," *IEEE Trans. Commun.*, vol. 64, no. 11, pp. 4836–4846, Nov. 2016.
[22] D. Darsena, G. Gelli, and F. Verde, "Modeling and performance analysis of wireless networks with ambient backscatter devices," *IEEE Trans. Commun.*, vol. 65, no. 4, pp. 1797–1814, Apr. 2017.
[23] X. Lu, H. Jiang, D. Niyato, D. I. Kim, and Z. Han, "Wireless powered device-to-device communications with ambient backscattering: Performance modeling and analysis," *IEEE Trans. Wireless Commun.*, vol. 17, no. 3, pp. 1528–1544, Mar. 2018.
[24] Q. Zhang, L. Zhang, Y.-C. Liang, and P.-Y. Kam, "Backscatter-NOMA: A symbiotic system of cellular and Internet-of-Things networks," *IEEE Access*, vol. 7, pp. 20000–20013, 2019.
[25] C. Yang, X. Wang, and K.-W. Chin, "On max–min throughput in backscatter-assisted wirelessly powered IoT," *IEEE Internet Things J.*, vol. 7, no. 1, pp. 137–147, Jan. 2020.
[26] Z. Ding, X. Lei, G. K. Karagiannidis, R. Schober, J. Yuan, and V. K. Bhargava, "A survey on non-orthogonal multiple access for 5G networks: Research challenges and future trends," *IEEE J. Sel. Areas Commun.*, vol. 35, no. 10, pp. 2181–2195, Oct. 2017.
[27] Y. Liu, Z. Qin, M. Elkashlan, Z. Ding, A. Nallanathan, and L. Hanzo, "Nonorthogonal multiple access for 5G and beyond," *Proc. IEEE*, vol. 105, no. 12, pp. 2347–2381, Dec. 2017.
[28] S. M. R. Islam, N. Avazov, O. A. Dobre, and K.-S. Kwak, "Power-domain non-orthogonal multiple access (NOMA) in 5G systems: Potentials and challenges," *IEEE Commun. Surveys Tuts.*, vol. 19, no. 2, pp. 721–742, 2nd Quart., 2017.
[29] Z. Yang, Z. Ding, P. Fan, and N. Al-Dhahir, "A general power allocation scheme to guarantee quality of service in downlink and uplink NOMA systems," *IEEE Trans. Wireless Commun.*, vol. 15, no. 11, pp. 7244–7257, Nov. 2016.
[30] H. Wang, R. Zhang, R. Song, and S.-H. Leung, "A novel power minimization precoding scheme for MIMO-NOMA uplink systems," *IEEE Commun. Lett.*, vol. 22, no. 5, pp. 1106–1109, May 2018.
[31] L. Zhu, J. Zhang, Z. Xiao, X. Cao, D. O. Wu, and X.-G. Xia, "Joint power control and beamforming for uplink non-orthogonal multiple access in 5G millimeter-wave communications," *IEEE Trans. Wireless Commun.*, vol. 17, no. 9, pp. 6177–6189, Sep. 2018.
[32] H. Wang, Y. Fu, R. Song, Z. Shi, and X. Sun, "Power minimization precoding in uplink multi-antenna NOMA systems with jamming," *IEEE Trans. Green Commun. Netw.*, vol. 3, no. 3, pp. 591–602, Sep. 2019.
[33] P. D. Diamantoulakis, Z. Ding, G. K. Karagiannidis, and K. N. Pappi, "Wireless-powered communications with non-orthogonal multiple access," *IEEE Trans. Wireless Commun.*, vol. 15, no. 12, pp. 8422–8436, Dec. 2016.
[34] H. Chingoska, Z. Hadzi-Velkov, I. Nikoloska, and N. Zlatanov, "Resource allocation in wireless powered communication networks with non-orthogonal multiple access," *IEEE Wireless Commun. Lett.*, vol. 5, no. 6, pp. 684–687, Dec. 2016.
[35] M. Zheng, W. Liang, and H. Yu, "Utility-based resource allocation in wireless-powered communication networks," *IEEE Syst. J.*, vol. 12, no. 4, pp. 3881–3884, Dec. 2018.
[36] Z. Chang, L. Lei, H. Zhang, T. Ristaniemi, S. Chatzinotas, B. Ottersten, and Z. Han, "Energy-efficient and secure resource allocation for multiple-antenna NOMA with wireless power transfer," *IEEE Trans. Green Commun. Netw.*, vol. 2, no. 4, pp. 1059–1071, Dec. 2018.
[37] C. Lee and Y. H. Kim, "Receive beamforming and resource allocation for wireless powered non-orthogonal multiple access," *IEEE Trans. Veh. Technol.*, vol. 69, no. 4, pp. 4563–4568, Apr. 2020.
[38] J. Guo, X. Zhou, S. Durrani, and H. Yanikomeroglu, "Design of non-orthogonal multiple access enhanced backscatter communication," *IEEE Trans. Wireless Commun.*, vol. 17, no. 10, pp. 6837–6852, Oct. 2018.
[39] G. Yang, X. Xu, and Y.-C. Liang, "Resource allocation in NOMA-enhanced backscatter communication networks for wireless powered IoT," *IEEE Wireless Commun. Lett.*, vol. 9, no. 1, pp. 117–120, Jan. 2020.
[40] Y. Liao, G. Yang, and Y.-C. Liang, "Resource allocation in NOMA-enhanced full-duplex symbiotic radio networks," *IEEE Access*, vol. 8, pp. 22709–22720, Jan. 2020.
[41] C. Qin, W. Ni, H. Tian, and R. P. Liu, "Joint rate maximization of downlink and uplink in multiuser MIMO SWIPT systems," *IEEE Access*, vol. 5, pp. 3750–3762, Mar. 2017.
[42] Z. Wen, Z. Guo, N. C. Beaulieu, and X. Liu, "Robust beamforming design for multi-user MISO full-duplex SWIPT system with channel state information uncertainty," *IEEE Trans. Veh. Technol.*, vol. 68, no. 2, pp. 1942–1947, Feb. 2019.
[43] Q. Qi, X. Chen, and D. W. K. Ng, "Robust beamforming for NOMA-based cellular massive IoT with SWIPT," *IEEE Trans. Signal Process.*, vol. 68, pp. 211–224, 2020.
[44] L. Liu, R. Zhang, and K.-C. Chua, "Multi-antenna wireless powered communication with energy beamforming," *IEEE Trans. Commun.*, vol. 62, no. 12, pp. 4349–4361, Dec. 2014.
[45] L.-N. Tran, M. F. Hanif, and M. Juntti, "A conic quadratic programming approach to physical layer multicasting for large-scale antenna arrays," *IEEE Signal Process. Lett.*, vol. 21, no. 1, pp. 114–117, Jan. 2014.
[46] S. Boyd and L. Vandenberghe, *Convex Optimization*. Cambridge, U.K.: Cambridge Univ. Press, 2004.

GERARDO SACARELO received the B.S.E. degree in electronics and telecommunications engineering from the Escuela Superior Politécnica del Litoral (ESPOL), Ecuador, in 2014. He is currently pursuing the combined M.S.-Ph.D. degree in electronic engineering with Kyung Hee University, South Korea. His research interests include cooperation communication, massive MIMO, and wireless powered communication with energy harvesting.

YUN HEE KIM (Senior Member, IEEE) received the B.S.E. *(summa cum laude)*, M.S.E., and Ph.D. degrees in electrical engineering from the Korea Advanced Institute of Science and Technology, Daejeon, South Korea, in 1995, 1997, and 2000, respectively. In 2000 and 2011, she was with the Department of Electrical and Computer Engineering, University of California at San Diego, San Diego, CA, USA, as a Visiting Researcher. From September 2000 to August 2004, she was with the Electronics and Telecommunications Research Institute, Daejeon, as a Senior Member of Research Staff. In September 2004, she joined the Department of Electronic Engineering, Kyung Hee University, Yongin, South Korea, where she is currently a Professor. Her research interests include wireless/mobile communications, statistical signal processing, and the ultra-low power Internet-of-Things.